Supporting Information

Nanoscale probing and imaging of HIV-1 RNA in cells with a chimeric LNA-DNA sensor

Alessia Amodio,[†a,b] Marco Cassani,[†a,c] Liviana Mummolo,[a] Christina Cortez-Jugo,[a] Sukhvir Kaur Bhangu,[d] Jori Symons,[e] Chantelle L. Ahlenstiel,[f] Giancarlo Forte,[c] Francesco Ricci,[b] Anthony D. Kelleher,[f] Sharon R. Lewin,[e,g,h] Francesca Cavalieri[b,d] and Frank Caruso*[a]*

[a]Department of Chemical Engineering, The University of Melbourne, Parkville, Victoria 3010, Australia

[b]Dipartimento di Scienze e Tecnologie Chimiche, Università degli Studi di Roma Tor Vergata, Via della Ricerca Scientifica 1, 00133 Rome, Italy

[c]International Clinical Research Center (ICRC), St Anne's University Hospital, CZ-65691 Brno, Czech Republic

[d]School of Science, RMIT University, Victoria 3000, Australia

[e]Department of Infectious Diseases, The University of Melbourne at the Peter Doherty Institute for Infection and Immunity, Melbourne, Victoria 3000, Australia

[f]Kirby Institute, University of New South Wales, New South Wales 2052, Australia

[g]Victorian Infectious Diseases Service, Royal Melbourne Hospital at the Peter Doherty Institute for Infection and Immunity, Melbourne, Victoria 3000, Australia

[h]Department of Infectious Diseases, Alfred Hospital and Monash University, Melbourne, Victoria 3004, Australia

*Corresponding authors. E-mail: francesca.cavalieri@rmit.edu.au; fcaruso@unimelb.edu.au

[†]A.A. and M.C. contributed equally to this work.

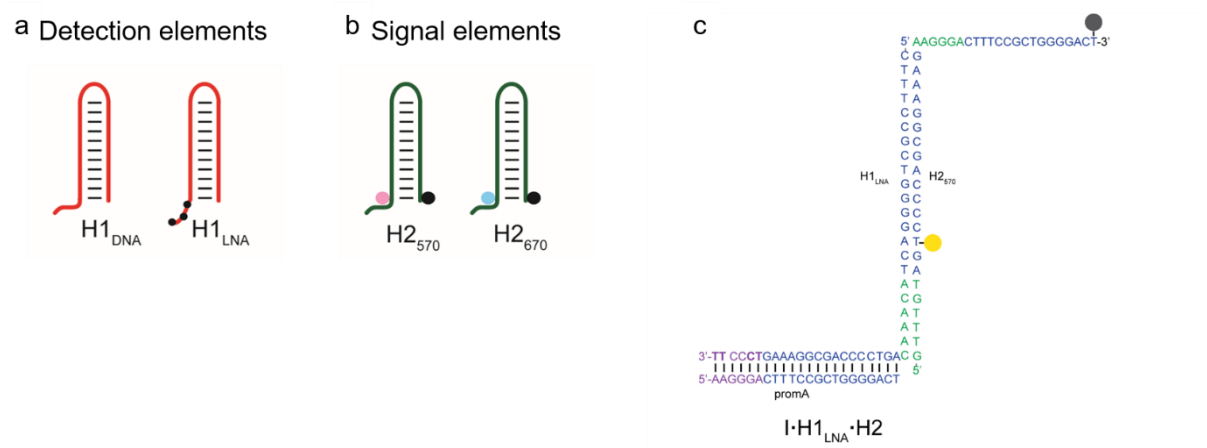

Figure S1 – Schematic depiction of HCR mechanism. (a) Detection elements: $H1_{DNA}$ and $H1_{LNA}$ – the detection elements have different sticky end domains. (b) Signal elements: DNA hairpin (H2) – the LNA bases in the toehold domain of $H1_{LNA}$ are represented by a black circle, whereas QUASAR® 570 in $H2_{570}$ is represented by a light pink circle and QUASAR® 670 in $H2_{670}$ is represented by a light blue circle. (c) Complex $I{\cdot}H1_{LNA}{\cdot}H2$.

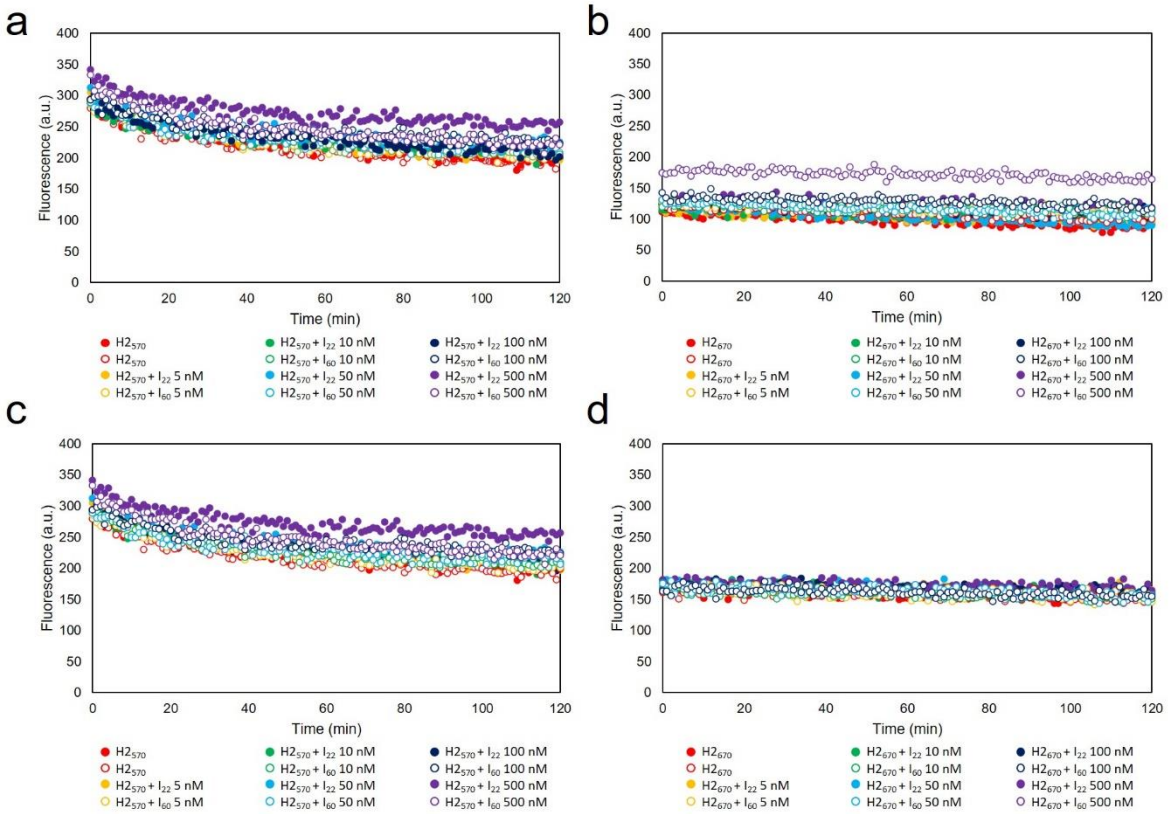

Figure S2 – Stability of H2 in the presence of I_{22} and *I_{60}. (a) Fluorescence signal as a function of time of $H2_{570}$ in PBS; $H2_{570}$ + I_{22} at varying concentrations of I_{22} (5, 10, 50, 100, and 500 nM); and $H2_{570}$ + I_{60} at varying concentrations of I_{60} (5, 10, 50, 100, and 500 nM). (b) Fluorescence signal as a function of time of $H2_{670}$ in PBS; $H2_{670}$ + I_{22} at varying concentrations of I_{22} (5, 10, 50, 100, and 500 nM); and $H2_{670}$ + I_{60} at varying concentrations of I_{60} (5, 10, 50, 100, and 500 nM). (c) Fluorescence signal as a function of time of $H2_{570}$ in PBS_PEG; $H2_{570}$ + I_{22} at varying concentrations of I_{22} (5, 10, 50, 100, and 500 nM); and $H2_{570}$ + I_{60} at varying concentrations of I_{60} (5, 10, 50, 100, and 500 nM). (d) Fluorescence signal as a function of time $H2_{670}$ in PBS_PEG; $H2_{670}$ + I_{22} at varying concentrations of I_{22} (5, 10, 50, 100, and 500 nM); and $H2_{670}$ + I_{60} at varying concentrations of I_{60} (5, 10, 50, 100, and 500 nM). The concentration of the hairpins (H2) in the reaction mixtures was constant (100 nM). The reaction kinetics was followed for 2 h at 37 °C.*

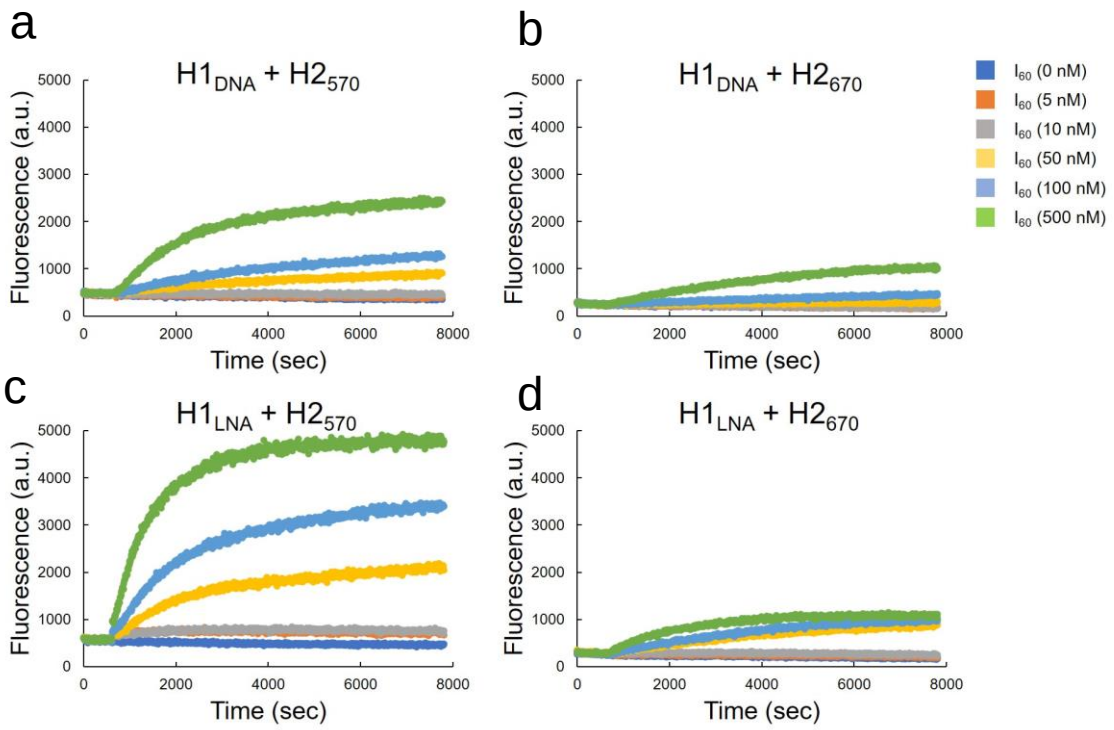

Figure S3 – HCR kinetics. Fluorescence signal as a function of time of different reaction mixtures at varying concentrations of I_{60} (0, 5, 10, 50, 100, and 500 nM): (a) $H1_{DNA}$ + $H2_{570}$; (b) $H1_{DNA}$ + $H2_{670}$; (c) $H1_{LNA}$ + $H2_{570}$; and (d) $H1_{LNA}$ + $H2_{670}$. The concentration of the hairpins (H1 and H2) in the reaction mixtures was constant (100 nM). The kinetics was followed for about 2 h at 37 °C.

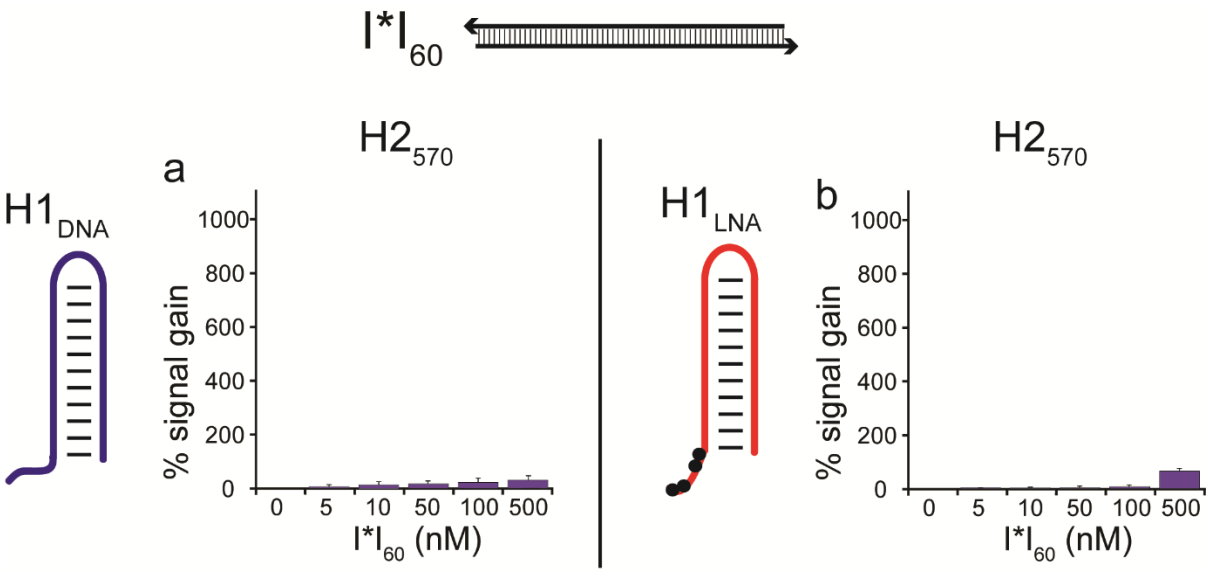

Figure S4 – Efficiency of the HCR reaction using initiator I^*I_{60}. Signal increase as a function of I^*I_{60} concentration using $H2_{570}$ for the two detection elements (a) $H1_{DNA}$ and (b) $H1_{LNA}$. The concentration of the hairpins (H1 and H2) in the reaction mixtures was constant (100 nM). The reactions were performed in PBS pH 7.4 and incubated for 2 h at 37 °C. (Values are shown as mean ± SD, averaged over at least three independent measurements).

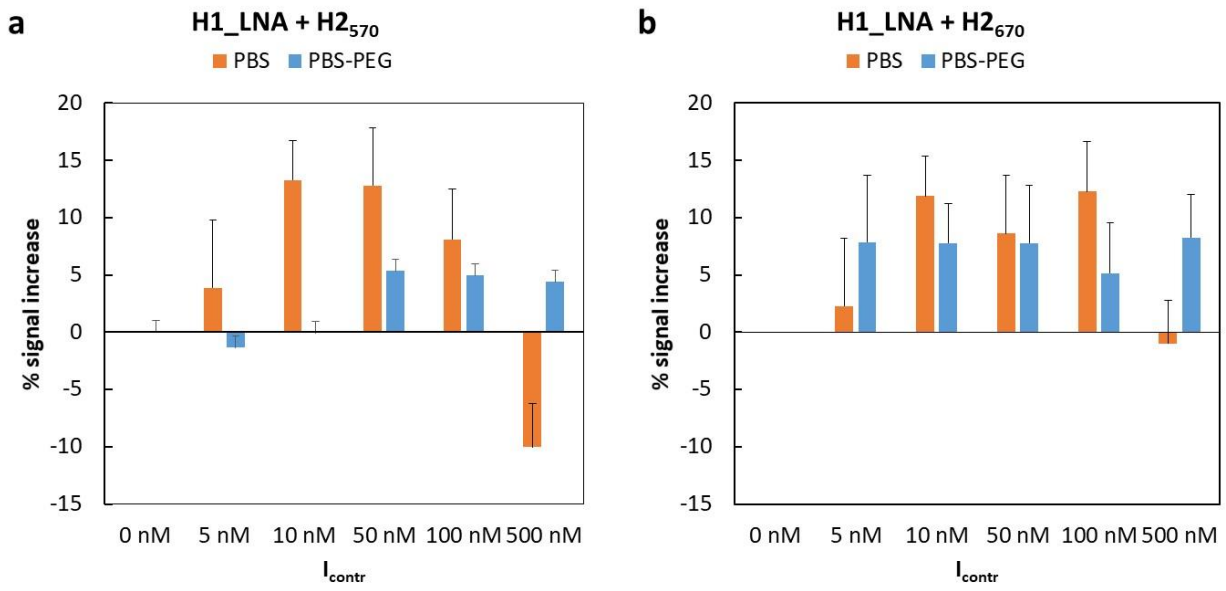

Figure S5 – The specificity of (a) $H1_{LNA}$ + $H2_{570}$ and (b) $H1_{LNA}$ + $H2_{670}$ was tested by using as Initiator a control sequence 5′-GGGACTTTCCTAGAAATTAT 3′ (I_{contr}) containing half bases similar to the target sequence PromA and half scrambled bases.

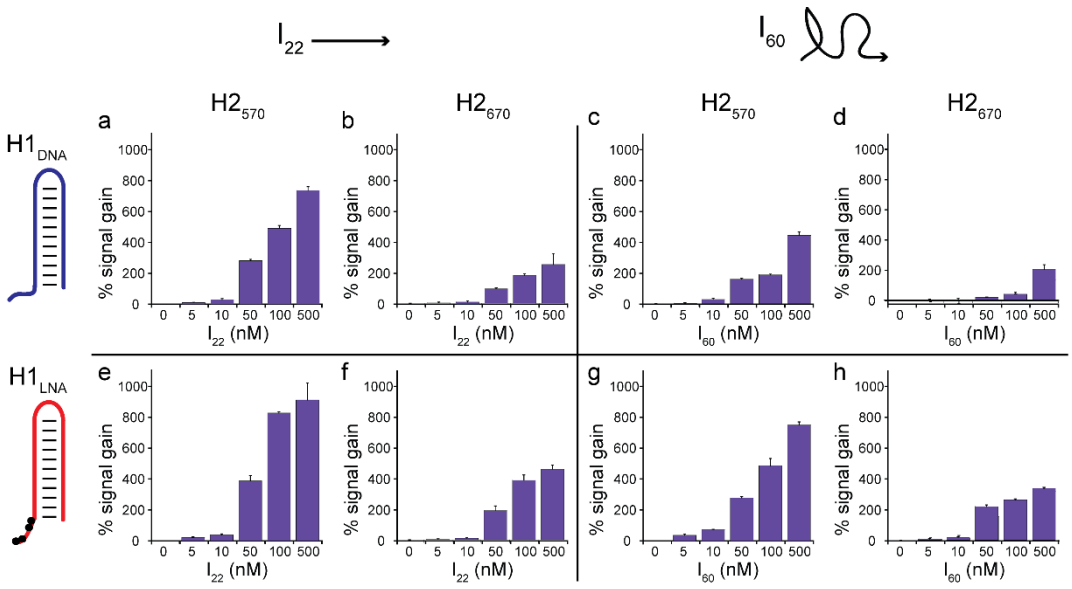

Figure S6 – Efficiency of the HCR reaction using initiators I_{22} and I_{60}. Signal increase as a function of I_{22} concentration using $H2_{570}$ for the two detection elements (a) $H1_{DNA}$ and (e) $H1_{LNA}$ or using $H2_{670}$ for the two detection elements (b) $H1_{DNA}$ and (f) $H1_{LNA}$. Signal increase as a function of I_{60} concentration using $H2_{570}$ for the two detection elements (c) $H1_{DNA}$ and (g) $H1_{LNA}$ or using $H2_{670}$ for the two detection elements (d) $H1_{DNA}$ and (h) $H1_{LNA}$. The concentration of the hairpins (H1 and H2) in the reaction mixtures was constant (100 nM). The reactions were performed in PBS + 30% w/v PEG_{3350}, pH 7.4 and incubated for 2 h at 37 °C. The values shown represent averages of at least three independent measurements; error bars reflect standard deviations.

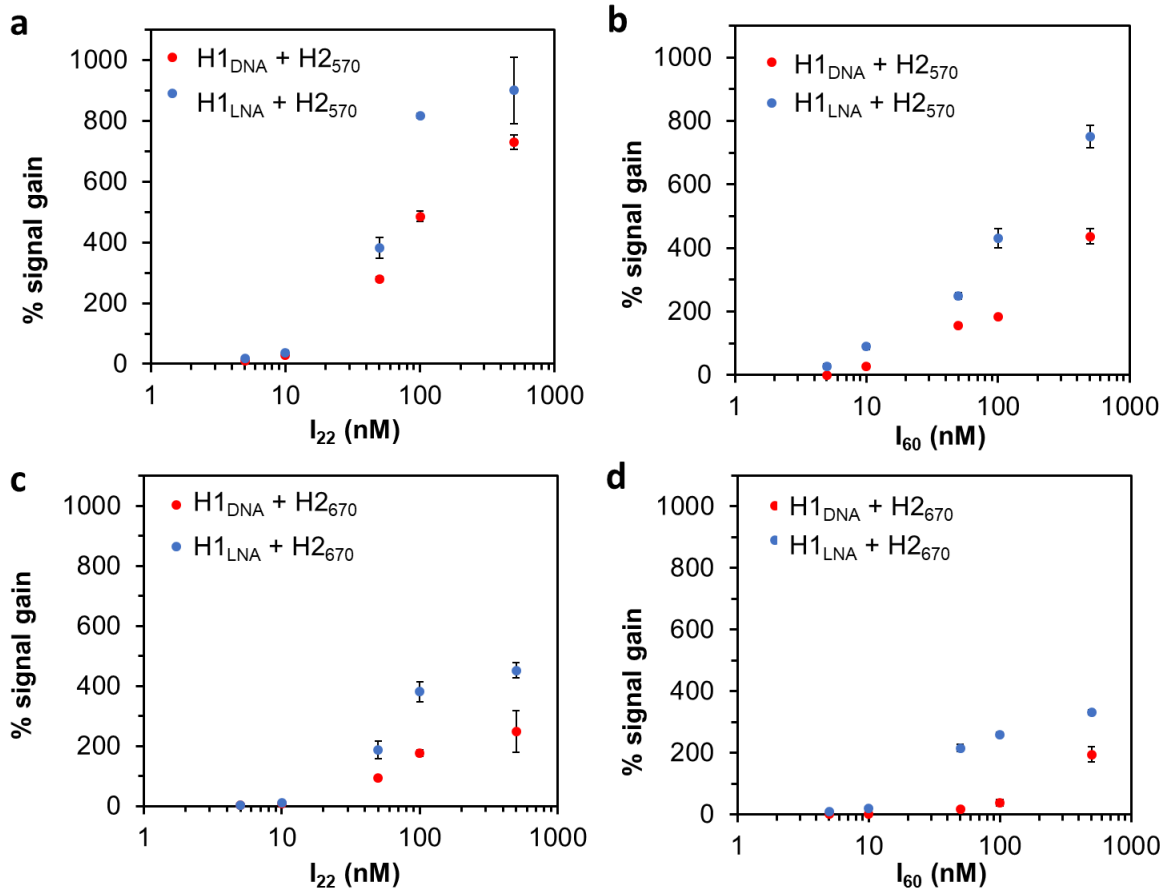

Figure S7 – Comparison of the efficiency of the HCR reaction shown in Figure S6 using a log scale. (a) Signal increase as a function of I_{22} concentration using $H2_{570}$ for the two detection elements. (b) Signal increase as a function of I_{60} concentration using $H2_{570}$ for the two detection elements. (c) Signal increase as a function of I_{22} concentration using $H2_{670}$ for the two detection elements. (d) Signal increase as a function of I_{60} concentration using $H2_{670}$ for the two detection elements.

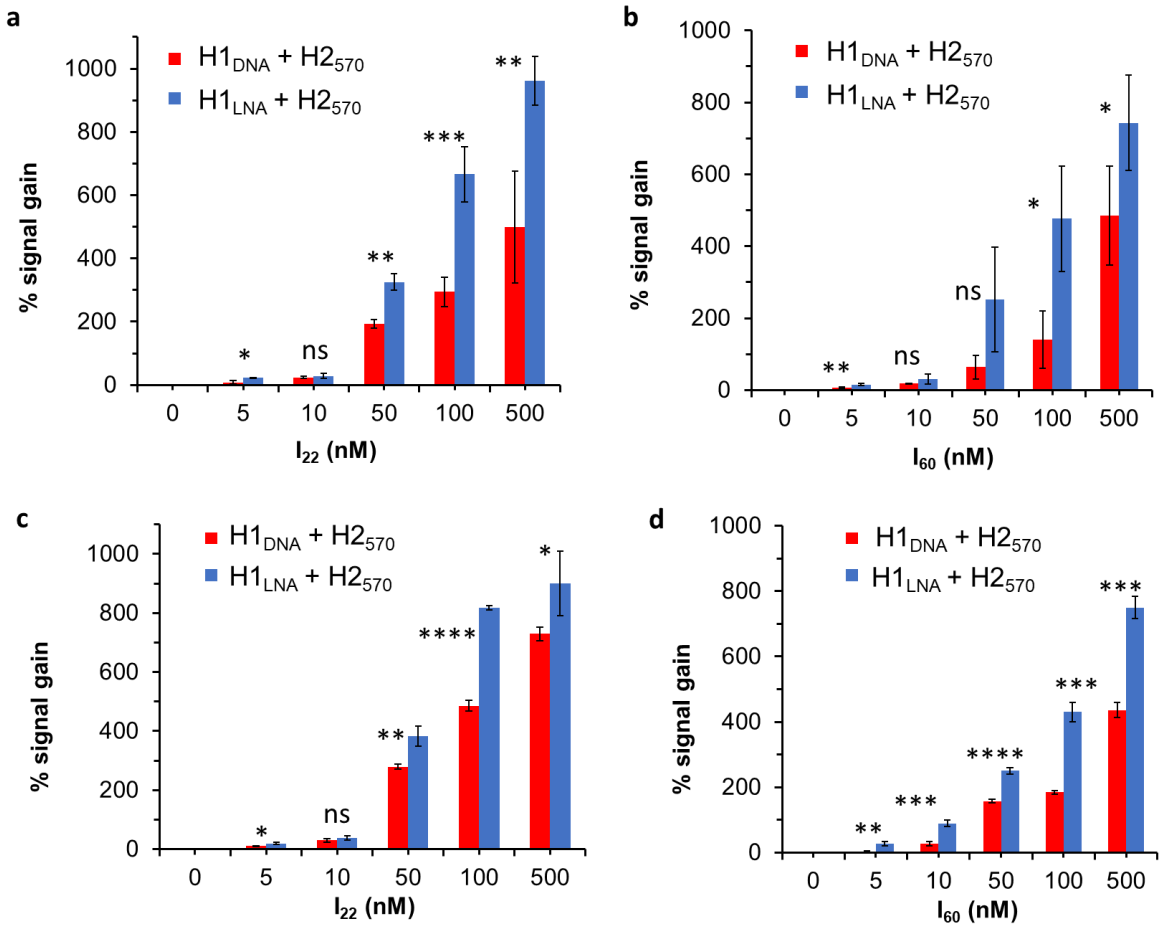

*Figure S8– Comparison of signal gains as a function of I_{22} and I_{60} concentrations:(a) $H1_{DNA}$ + $H2_{570}$ + I_{22} and $H1_{LNA}$ + $H2_{570}$ + I_{22} and (b) $H1_{DNA}$ + $H2_{570}$ + I_{60} and $H1_{LNA}$ + $H2_{570}$+ I_{60}. The concentration of the hairpins ($H1_{DNA}$, $H1_{LNA}$, and $H2_{570}$) in the reaction mixtures was constant (100 nM). The reactions were performed in PBS, pH 7.4 and incubated for 2 h at 37 °C. (c) $H1_{DNA}$ + $H2_{570}$ + I_{22} and $H1_{LNA}$ + $H2_{570}$ + I_{22} and (d) $H1_{DNA}$ + $H2_{570}$ + I_{60} and $H1_{LNA}$ + $H2_{570}$ + I_{60}. The concentration of the hairpins ($H1_{DNA}$, $H1_{LNA}$, and $H2_{570}$) in the reaction mixtures was constant (100 nM). The reactions were performed in PBS+ 30% w/v PEG_{3350}, pH 7.4 and incubated for 2 h at 37 °C. ns non-significant, **** p-value ≤ 0.0001, *** p-value ≤ 0.001, ** p-value ≤ 0.01, * p-value ≤ 0.05 as calculated using one-way ANOVA with 95% confidence interval and Tukey's pairwise comparison.*

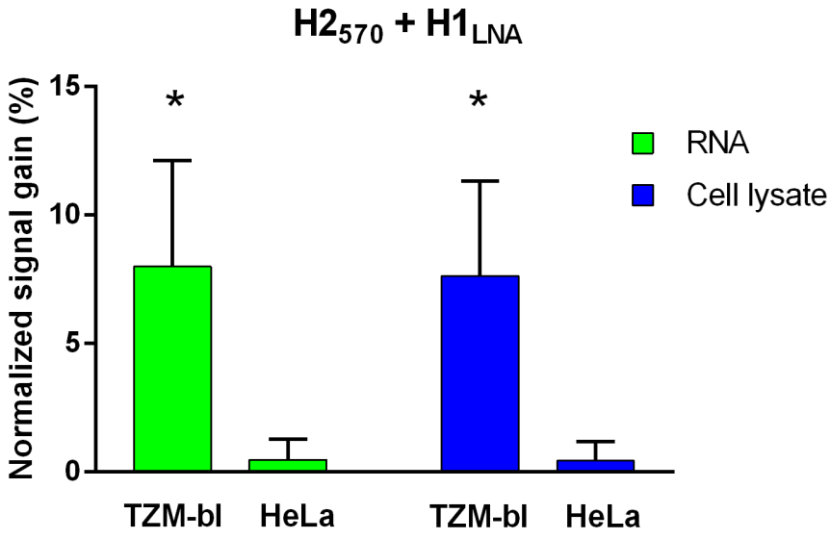

*Figure S9 – HCR in vitro. Signal gain of HCR reaction in RNA extracted from HeLa and TZM-bl cells and in cell lysate of HeLa and TZM-bl cells. (Two-way ANOVA followed by post-hoc Sidak, * indicates $p < 0.05$).*

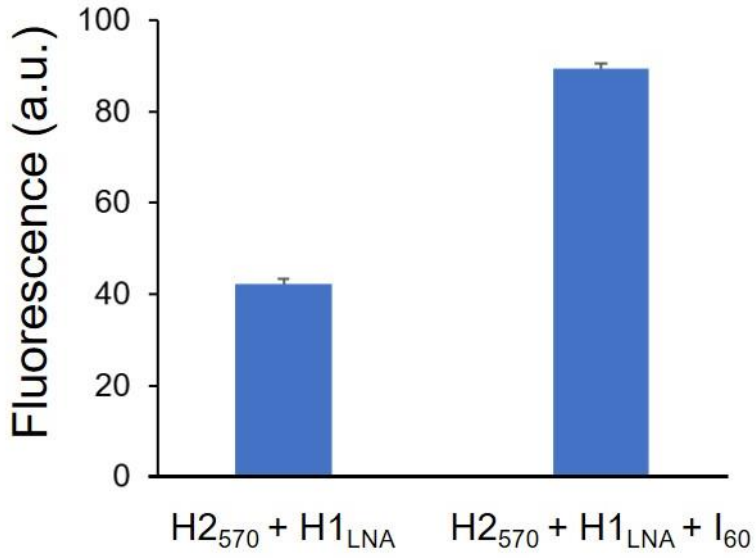

Figure S10 – Stability of $H2_{570}$ + $H1_{LNA}$ upon complexation with lipofectamine, with and without I_{60}. The experiment was performed using $H1_{LNA}$ (20 nM), $H2_{570}$ (20 nM), and I_{60} (10 nM). Both reaction mixtures were incubated overnight at room temperature, and the samples were analyzed using a fluorometer.

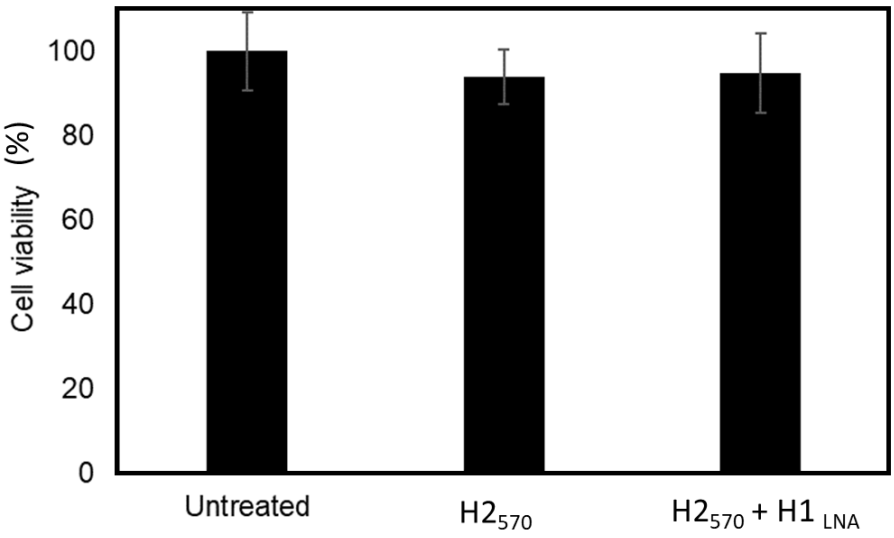

Figure S11 – Relative viability of TZM-bl cells after 4 h transfection with lipofectamine-$H2_{570}$ only or lipofectamine-$H2_{570}$ + $H1_{LNA}$ complexes as measured by an XTT assay. The viability of untreated cells was set at 100%.

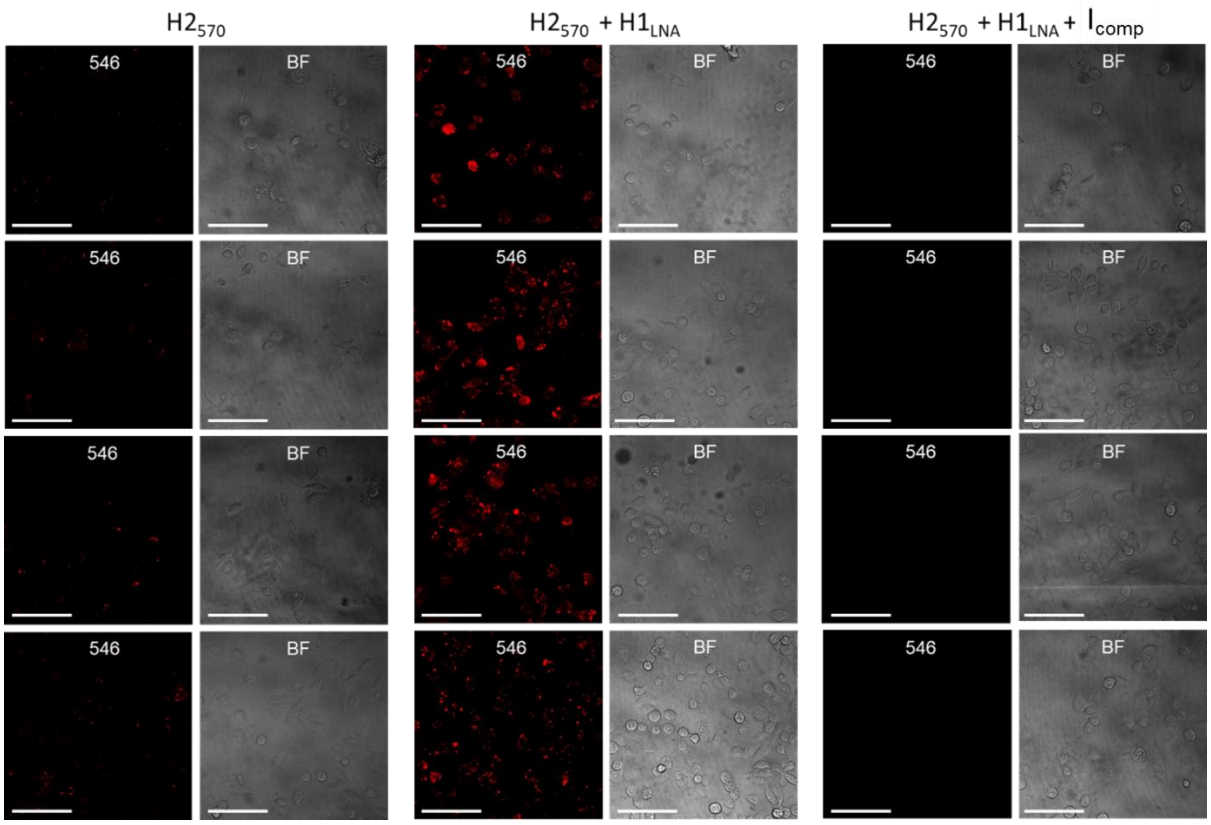

Figure S12 – Live confocal microscopy imaging of TZM-bl cells incubated with $H2_{570}$ only (left), $H2_{570}$ + $H1_{LNA}$ (middle), or $H2_{570}$ + $H1_{LNA}$ + inhibitor I_{comp} (right). Excitation wavelength, λ_{ex}, is 546 nm. Scale bars are 100 µm. The rows indicate images from four representative field of views.

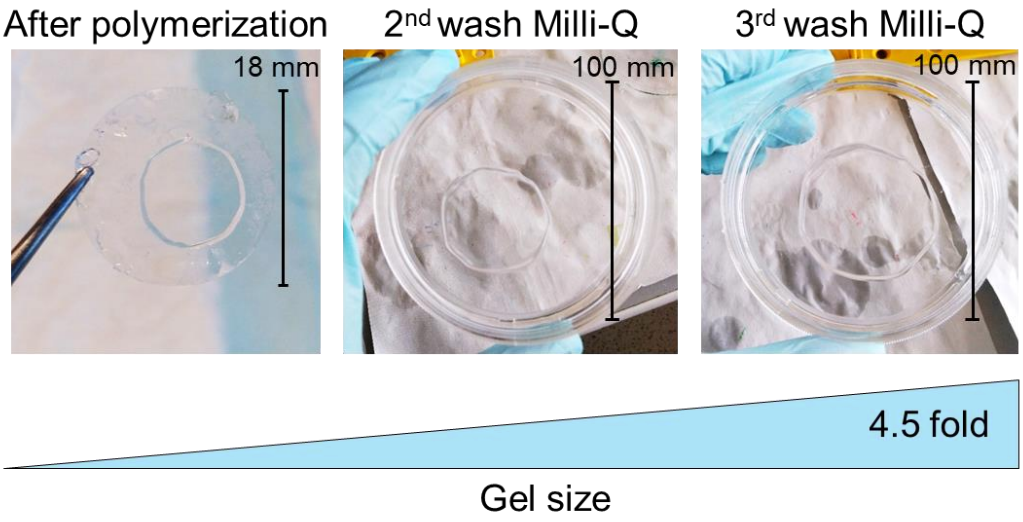

Figure S13 – Size of hydrogel as a function of the washing conditions employed.

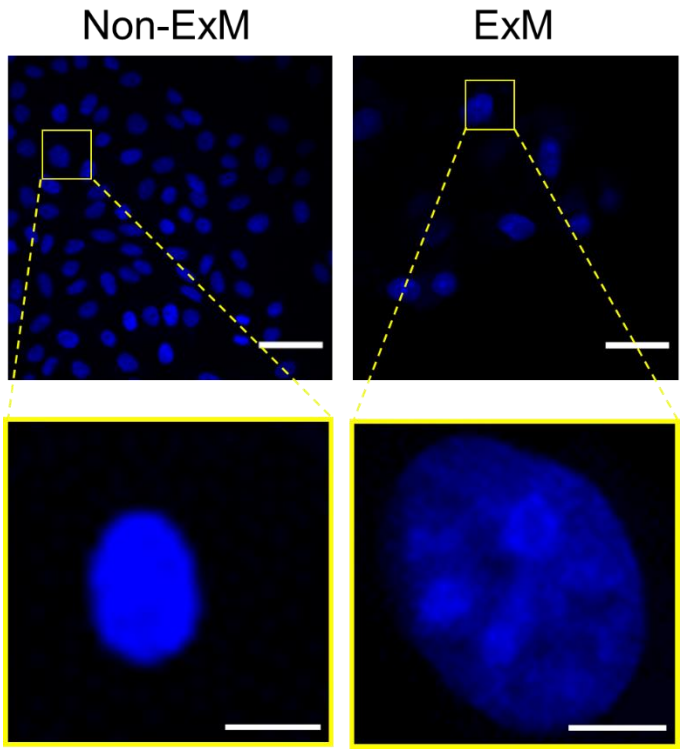

Figure S14 – CLSM images of nuclei from fixed non-expanded and expanded TZM-bl cells at low and high magnification. Nuclei were stained with DAPI. λ_{ex} = 405 nm. Scale bars are 50 µm and 10 µm in the low- and high-magnification images, respectively (expansion factor 3.8×).

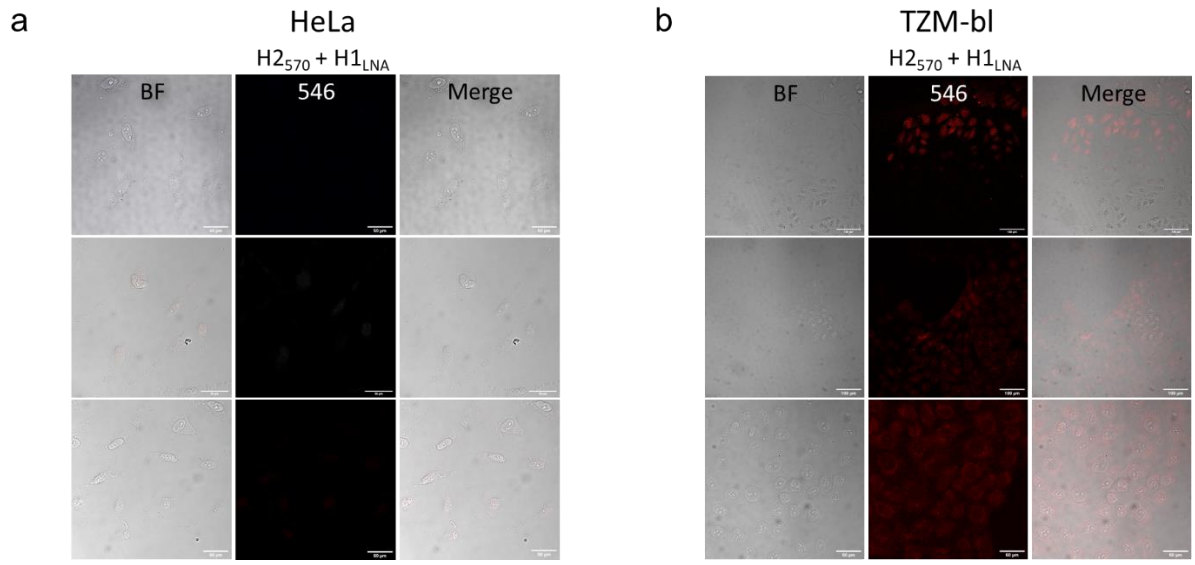

Figure S15 – CLSM images of (a) HeLa and (b) TZM-bl cells subjected to ExM procedure involving incubation with $H2_{570}$ + $H1_{LNA}$. Bright-field (BF) images and images showing cells excited with λ_{ex} = 546 nm (546) are presented. Scale bars are 50 μm in (a) and (b) (expansion factor 2.3×).

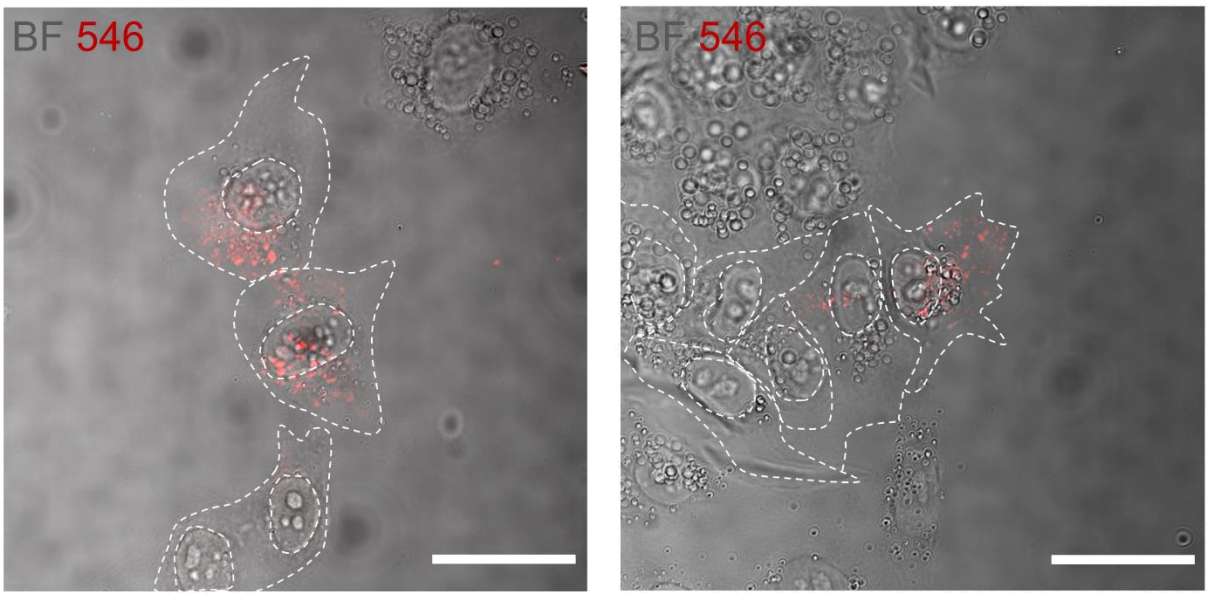

Figure S16 – Confocal microscopy images showing the overlap of BF and 546 channels of the expanded cells showed in Figure 5. The dashed lines indicate the outlines of the outer membranes and nuclear membranes of cells. Scale bars are 50 μm (expansion factor 2.3×).

a

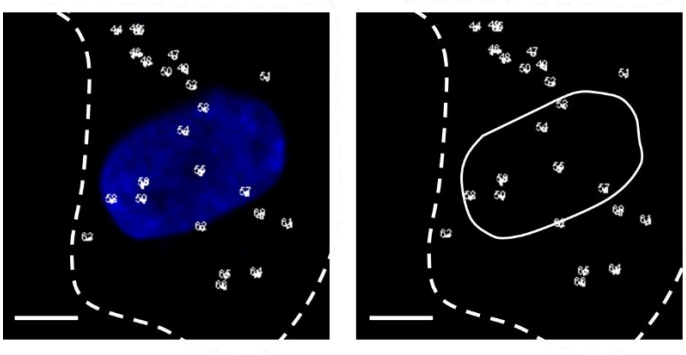

b

HCR loci area (μm^2)	HCR loci per cell
MAX: 2.4 μm^2 **MIN: 0.1 μm^2**	33 ± 20

Figure S17 – Determination of HCR spots location inside the cells. (a) Representative images of HCR spots in TZM-b cell detected with the applied threshold size (0.2–0.8 μm^2) using Fiji software. Nuclei are stained in blue. The dashed lines indicate the cell and the solid line indicates the nucleus. Scale bars in (a) are 10 μm (expansion factor 2.3×). (b) Average area per HCR loci and average number of HCR loci per cells (N >100 cells).

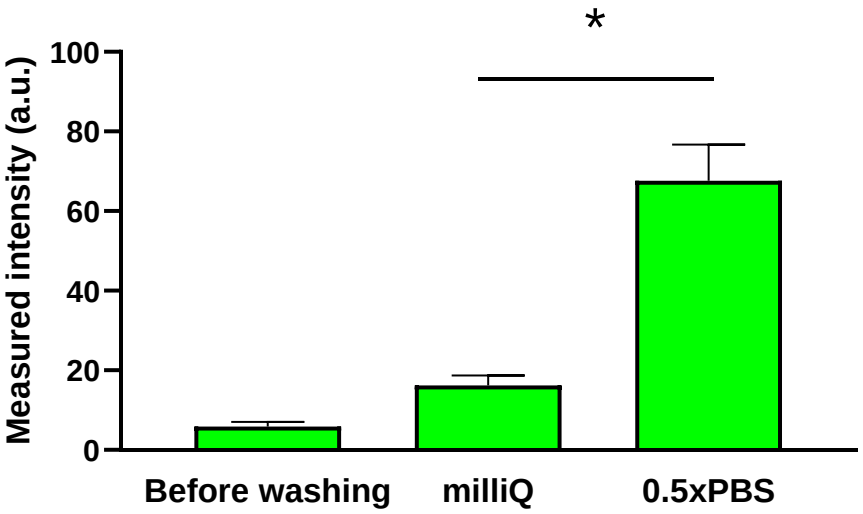

*Figure S18 – Bar plot of Dx-FITC signal intensity of the expanded TZM-bl cells sample before and after washing in Milli-Q water or 0.5× PBS. The values are normalized taking into account the dilution factor, expressed as volume increase following hydrogel expansion. Independent t-test, N > 50 cells. * indicates $p < 0.0001$.*

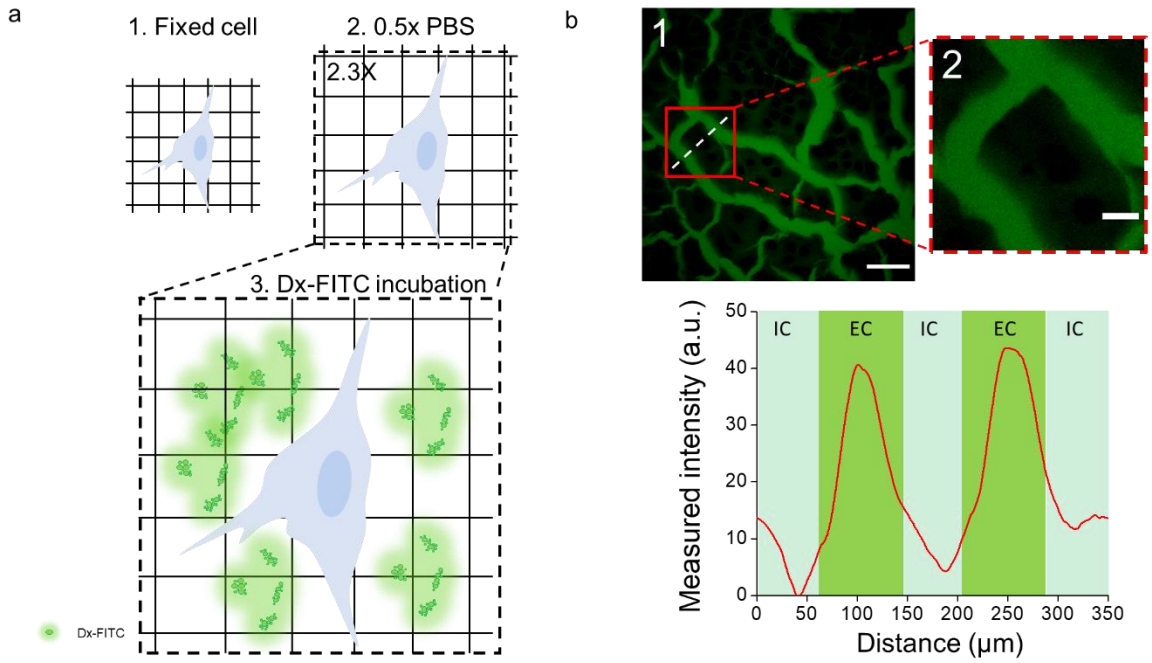

Figure S19 – Extracellular hydrogel mesh size evaluation with standard dextran-FITC (a) Schematic of the post-expansion incubation of hydrogel-containing cells with Dx-FITC. Cells were first fixed (1.), then expanded and washed with 0.5× PBS (2.) and finally incubated with Dx-FITC for 2 h (3.). (b) CLSM images (top) of the hydrogel containing TZM-bl cell sample incubated with Dx-FITC after expansion. Red box indicates the magnified area as shown on the right. λ_{ex} *= 488 nm. Scale bars are 100 µm (expansion factor is 2.3× (b1)) and 25 µm (expansion factor is 2.3× (b2)), respectively. Intensity plot (bottom) of the green signal measured for the area of the hydrogel picture marked with a dashed white line in the top section of panel b.*

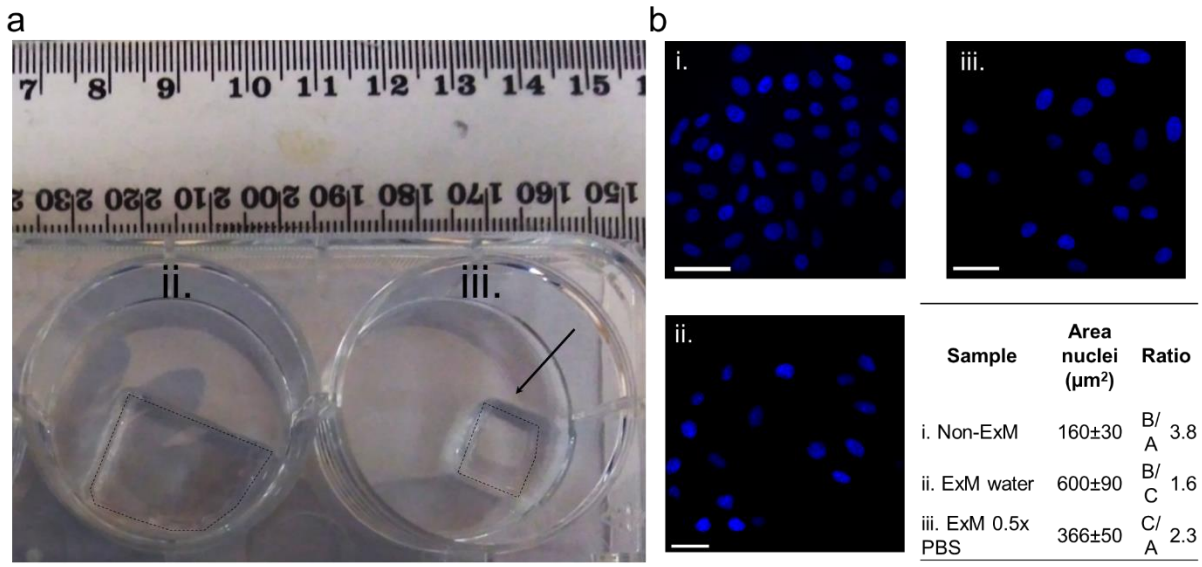

Sample	Area nuclei (μm²)	Ratio	
i. Non-ExM	160±30	B/A	3.8
ii. ExM water	600±90	B/C	1.6
iii. ExM 0.5x PBS	366±50	C/A	2.3

Figure S20 – Characterization of hydrogel expansion and nuclei size in hypotonic conditions. (a) Photograph of hydrogels treated under two different conditions (ExM water (ii) and ExM 0.5× PBS (iii)). Dotted lines indicate the outline (dimension) of the gels. The black arrow indicates the change in the dimension of the hydrogel washed with 0.5× PBS compared with the hydrogel washed with Milli-Q water. (b) CLSM images of DAPI nuclei staining for fixed cells in non-swollen gel (i.), cells expanded in water (ii.) and cells expanded and washed with 0.5× PBS (iii.). λ_{ex} = 405 nm. Scale bars are 50 μm (expansion factors are 3.8× (b ii.) and 2.3× (b iii.)). (Values and relative ratios of the nuclei area determined from the CLSM images are tabulated. The size of the nuclei was determined using Fiji software).

Table S1 *– Comparison of sensitivity limits for different techniques used for the detection of HIV-1*

Reference	Detection limit of HIV-1 DNA/RNA	System
This work	8–15 nM	HCR
[1]	10 fM	Gold nanoclusters/graphene electrode
[2, 3]	10 copies	Recombinase polymerase amplification (RPA)
[4]	78 copies/mL	Simple amplification-based assay (SAMBA)
[5]	10^6 copies/mL	Loop-mediated isothermal amplification (LAMP)
[6]	57 copies/mL	PCR
[7]	50 copies	Microfluidic-PCR assay
[8]	5 copies/μL	Microfluidic-PCR assay
[9]	45 cells/million	RNAscope

Table S2 *– Analysis of sensitivity of the HCR probes in PBS and PBS + PEG*

Sample (PBS)	Sensitivity (signal gain %/nM)	LOD* (nM)	Sample (PBS + 30% w/v PEG_{3350})	Sensitivity (signal gain %/nM)	LOD* (nM)
$H1_{DNA} + H2_{570} + I_{22}$	3.8	39	$H1_{DNA} + H2_{570} + I_{22}$	5.45	9
$H1_{LNA} + H2_{570} + I_{22}$	6.8	15	$H1_{LNA} + H2_{570} + I_{22}$	7.75	9
$H1_{DNA} + H2_{670} + I_{22}$	1.7	13	$H1_{DNA} + H2_{670} + I_{22}$	3.80	33
$H1_{LNA} + H2_{670} + I_{22}$	3.5	10	$H1_{LNA} + H2_{670} + I_{22}$	6.35	11
$H1_{DNA} + H2_{570} + I_{60}$	1.2	16	$H1_{DNA} + H2_{570} + I_{60}$	3.10	8
$H1_{LNA} + H2_{570} + I_{60}$	4.9	8	$H1_{LNA} + H2_{570} + I_{60}$	5.15	8
$H1_{DNA} + H2_{670} + I_{60}$	0.1	48	$H1_{DNA} + H2_{670} + I_{60}$	0.35	17
$H1_{LNA} + H2_{670} + I_{60}$	3.1	7	$H1_{LNA} + H2_{670} + I_{60}$	4.20	10

The sensitivity of the HCR probes determined in PBS was calculated from the slope of the linear regions obtained in the lower concentration range of data shown in Figures 2 a–h and S8. *Limit of detection (LOD) was calculated as LOD = 3 (standard deviation of the intercept/slope of the linear region).

Table S3 – *The experimental procedure used to assess HCR in live TZM-bl cells*

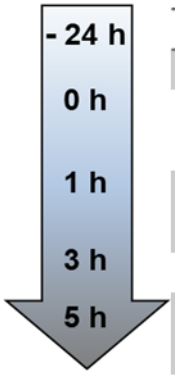

$H2_{570}$	**$H2_{570}$ + $H1_{LNA}$**	**I_{comp} + $H2_{570}$ + H1LNA**
1. Cell seeding	1. Cell seeding	1. Cell seeding
2. Medium replacement	2. Medium replacement	2. Medium replacement and **I_{comp} transfection**
3. $H2_{570}$ transfection	**3. $H2_{570}$ and $H1_{LNA}$ transfection**	**3. $H2_{570}$ and $H1_{LNA}$ transfection**
4. Medium replacement	4. Medium replacement	4. Medium replacement
5. Confocal microscopy analysis	5. Confocal microscopy analysis	5. Confocal microscopy analysis

References

1 Y. Wang, X. Bai, W. Wen, X. Zhang, S. Wang, *ACS Appl. Mater. Interfaces*, 2015, **7**, 18872.
2 M. Mansfield, in *Lateral Flow Immunoassay*, ed. R. Wong and H. Tse, Humana Press, Totowa, NJ, 2009, Ch. 6, pp. 95–113.
3 B. A. Rohrman, R. R. Richards-Kortum, *Lab Chip*, 2012, **12**, 3082.
4 H. H. Lee, M. A. Dineva, Y. L. Chua, A. V. Ritchie, I. Ushiro-Lumb, C. A. Wisniewski, *J. Infect. Dis.*, 2010, **201(Suppl)**, S65.
5 F. B. Myers, R. H. Henrikson, J. Bone, L. P. Lee, *PLoS One*, 2013, **8**, e70266.
6 S. Tanriverdi, L. Chen, S. Chen, *J. Infect. Dis.*, 2010, **201(Suppl)**, S52.
7 W. Tang, W. H. A. Chow, Y. Li, H. Kong, Y. W. Tang, B. Lemieux, *J. Infect. Dis.*, 2010, **201(Suppl)**, S46.
8 S. R. Jangam, A. K. Agarwal, K. Sur, D. M. Kelso, *Biosens. Bioelectron.*, 2013, **42**, 69.
9 W. Zhang, S. Svensson Akusjärvi, A. Sönnerborg, U. Neogi, *Front. Microbiol.*, 2018, **9**, 2358.